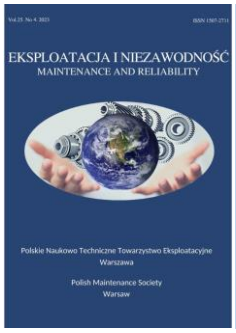

Eksploatacja i Niezawodnosc – Maintenance and Reliability
Volume 25 (2023), Issue 4
journal homepage: http://www.ein.org.pl

Article citation info:
Li J, Chen J, Zhang X, Wu Z, Time-dependent reliability analysis of corroded RC beams based on the phase-type fitting method, Eksploatacja i Niezawodnosc – Maintenance and Reliability 2023: 25(4) http://doi.org/10.17531/ein/172442

Time-dependent reliability analysis of corroded RC beams based on the phase-type fitting method

Indexed by:
Web of Science Group

Junxiang Li[a,b], Jianqiao Chen[c,d], Xinxin Zhang[a,b], Zijun Wu[a,b,*]

[a] Hubei Key Laboratory of Digital Textile Equipment, Wuhan Textile University, China
[b] School of Mechanical Engineering and Automation, Wuhan Textile University, China
[c] Department of Mechanics, Huazhong University of Science and Technology, China
[d] Hubei Key Laboratory for Engineering Structural Analysis and Safety Assessment, Huazhong University of Science and Technology, China

Highlights

- A novel phase-type (PH) fitting method is developed for time-dependent reliability.
- A reliability model of reinforced concrete beams is formulated by considering the time-dependent chloride diffusion coefficient.
- A new strategy is incorporated with Expectation Maximization algorithm to simply, efficiently and scientifically obtain the parameters of the PH method.
- The proposed method shows excellent computational efficiency and accuracy.

Abstract

It remains an important challenge to quantitatively describe the corrosion of reinforced concrete (RC) structures under chloride penetration. When considering the uncertainties encountered throughout the life cycle of RC structures exposed to a corrosive environment and evaluating their safety and reliability, the complexity of the problem intensifies. To address these issues, this paper focuses on the time-dependent reliability analysis of corroded RC beams, utilizing the phase-type (PH) fitting method. Initially, a model for the time-dependent reliability of corroded RC beams is established, incorporating the time-dependent chloride diffusion coefficient. Subsequently, a novel PH fitting method is proposed. The effectiveness of this new method is demonstrated through numerical examples. Furthermore, the time-dependent reliability analysis of corroded RC beams is compared using both the PH fitting method and the Monte Carlo simulation. The results reveal that the proposed method can accurately and efficiently deal with time-dependent reliability problems.

Keywords
chloride penetration, uncertainties, time-dependent reliability analysis, PH fitting method, corroded reinforced concrete beams.

1. Introduction

The corrosion of steel bars in concrete stands as a prominent determinant leading to the failure of reinforced concrete (RC) structures. The resultant damage to these structures can be categorized into two distinct types: concrete carbonation and chloride penetration [3, 18, 42, 53]. However, in practical engineering, the rate of chloride ion penetration surpasses that of concrete carbonation [63]. Hence, the chloride penetration has stronger impact on reinforcement corrosion and structural deterioration.

Two primary sources of chloride ions have been identified [22]: the first source involves the addition of chloride during the mixing and pouring phase, including calcium chloride and sodium chloride. The second source originates from the external environment during the service period, encompassing deicing salts used in winter, seawater, and sea breeze. Chlorides infiltrate the concrete through diffusion, driven by concentration gradients. Once the chloride concentration at the depth of a steel bar exceeds the chloride threshold level, the

(*) Corresponding author.
E-mail addresses: J. Li (ORCID: 0000-0003-0616-5335) jxli@wtu.edu.cn, J. Chen (ORCID: 0000-0003-3859-0299) jqchen@mail.hust.edu.cn, X. Zhang (ORCID: 0000-0002-3955-193X) xxzhang@wtu.edu.cn, Z. Wu (ORCID: 0000-0001-5020-5619) zjwu@wtu.edu.cn

protective passivation film on the surface of the steel bar deteriorates due to the combined effects of water, oxygen, and chloride [40, 46, 50]. Subsequently, corrosion occurs within the bar. The corrosion of steel reinforcements can lead to concrete fractures through cracking, delamination, and spalling of the concrete cover. Moreover, it results in a reduction in the cross-sectional area of both the concrete and reinforcements, significantly compromising the serviceability, strength, safety, and lifespan of concrete structures [44].

Fick's second law provides an effective description of chloride penetration in concrete. In 1972, Collepardi et al. [10] introduced a method for calculating the chloride diffusion coefficient based on Fick's second law, which subsequently gained widespread adoption [4, 8, 9, 13, 36, 56]. The chloride diffusion coefficient plays a pivotal role in the transportation of chlorides within concrete. Many diffusion models, rooted in Fick's second law, assume a constant value for the chloride diffusion coefficient [2, 10, 18, 44, 23]. However, in practical scenarios, particularly in marine environments, the diffusion of chloride ions into concrete exhibits nonlinear and time-dependent behavior [24, 61]. Consequently, the actual chloride diffusion coefficient varies over time, rather than remaining constant.

The performance of RC structures is influenced by various factors, including material properties and environmental conditions. Given the material heterogeneity, environmental complexity, and uncertainties associated with both, a probabilistic approach is necessary to study the corrosion damage of RC structures [62]. Additionally, when considering the time-dependent chloride diffusion coefficient and stochastic characteristics of loads, it is essential to perform time-dependent reliability analysis of RC structures. Saassouh and Lounis [44] used the first-order reliability method (FORM) and second-order reliability method (SORM) to predict the time-dependent probability of a RC highway bridge deck. El Hajj Chehade et al. [14] proposed a simplified time-dependent reliability model for a set of 21 simply supported RC T-beam bridges under variable traffic load considering the concrete creep and shrinkage. Some other related studies include Bagheri et al. [5], Guo et al. [20], Fan et al. [17] and Yang and Li [65].

Reliability is quantified as the integration of the irregular region in multidimensional space, and direct integration methods exhibit limited feasibility. For intricate reliability analysis problems, Monte Carlo simulation (MCS) [7, 67] stands as a potent and versatile technique. Its advantage lies in obtaining precise numerical solutions directly based on simulation test results. However, MCS entails a significant computational burden, which poses a major drawback. The FORM [66] and SORM [71] offer a relatively lower computational cost compared to MCS for evaluating reliability. Nonetheless, as the nonlinearity of the limit state function (LSF) increases, the approximate accuracy of these methods cannot be guaranteed [29].

The phase-type (PH) fitting method presents a substantial reduction in computational cost while ensuring reliability accuracy. Furthermore, this method possesses the advantageous property that any positive dataset can be approximated as a PH distribution using the Expectation Maximization (EM) algorithm. As a result, the PH fitting method has gained widespread usage in the field of reliability engineering [1, 12, 33, 57, 58]. However, previous studies have relied on trial methods [31] to determine relevant parameters, which involve a complex, inefficient, and unscientific operational process. Different from the original PH fitting method [31, 43, 55], the proposed novel method identifies the parameters in an automatic, efficient, and scientific iterative manner. The stopping criterion is adopted to simplify the process of parameter estimation.

Considering the limitations of the aforementioned research, this paper focuses on the time-dependent reliability analysis of corroded RC beams using the PH fitting method. The paper aims to achieve three primary objectives: 1) developing a reliability model for RC structures that incorporates the time-dependent chloride diffusion coefficient; 2) proposing a novel approach to obtain the parameters of the PH fitting method in a simple, efficient, and scientifically rigorous manner; 3) demonstrating the accurate and efficient application of the novel PH fitting method in handling time-dependent reliability analysis of corroded RC beams.

The paper is organized as follows. Section 2 establishes the framework for the time-dependent reliability analysis of corroded RC beams. Section 3 introduces the novel PH fitting method. In Section 4, the proposed methodology is validated through numerical examples and a case study involving

corroded RC beams. Finally, Section 5 presents the conclusions derived from this study.

2. Time-dependent reliability analysis of corroded RC beams

2.1. Review of time-dependent reliability analysis

In engineering applications, a multitude of uncertainties arises throughout the life cycle of structures, spanning the stages of design, construction, and operation. These uncertainties are commonly represented by random variables or stochastic processes. In the context of time-dependent reliability analysis, the general form of a LSF can be expressed as $G(\mathbf{X}, \mathbf{Y}(t), t)$, where $\mathbf{X}$ represents a vector of random variables, $\mathbf{Y}(t)$ denotes a vector of stochastic processes, and t signifies the time parameter. Over a specified time interval $[0, T_L]$, failure occurs if there exists a specific time instant t within $[0, T_L]$ where the LSF value falls below zero [26]:

$$\exists t \in [0, T_L], G(\mathbf{X}, \mathbf{Y}(t), t) \le 0 \quad (1)$$

As a result, the time-dependent probability of failure $P_f(0, T)$ over a time period $[0, T]$ $(0 \le T \le T_L)$ is a monotonically increasing function with respect to T. It can be defined as:

$$P_f(0,T) = Pr(\exists t \in [0,T], G(\mathbf{X}, \mathbf{Y}(t), t) \le 0), 0 \le T \le T_L \quad (2)$$

And time-dependent reliability is given by:

$$R(0,T) = Pr(\forall t \in [0,T], G(\mathbf{X}, \mathbf{Y}(t), t) > 0), 0 \le T \le T_L = 1 - P_f(0,T), 0 \le T \le T_L \quad (3)$$

2.2. Modeling of time-dependent reliability analysis for corroded RC beams

To simplify the problem, only the corrosion model for steel reinforcement bars is considered, without considering the corrosion model for concrete. This research is the foundation of our further works when the corrosion model for concrete is also taken into account.

The primary focus of this paper revolves around the corrosion phenomenon in RC beams caused by chloride ion attack. To describe the process of chloride penetration in concrete, Fick's second law is employed [44]:

$$\frac{\partial C(x,t)}{\partial t} = \frac{\partial}{\partial x}\left(D \frac{\partial C(x,t)}{\partial x}\right) \quad (4)$$

where x is the depth from the concrete surface; $C(x, t)$ is the concentration of chlorides at depth x and time t; D is the chloride diffusion coefficient.

In the case of a constant chloride diffusion coefficient D, and considering the following initial and boundary conditions, the Crank's solution can be derived [11]:

$$C(0,t) = C_s, C(x,0) = 0 \quad (5)$$

$$C(x,t) = C_s\left[1 - erf\left(\frac{x}{2\sqrt{Dt}}\right)\right] \quad (6)$$

$$erf(z) = 2\Phi(z\sqrt{2}) - 1 \quad (7)$$

where C_s is the surface chloride concentration, $erf()$ is the error function or Gauss error function.

In practical scenarios, the chloride diffusion coefficient may vary with time. For modeling the time-dependent chloride diffusion coefficient, a power law relationship is commonly recommended [32]:

With the cement hydration proceeding, the concrete pore structure is refined and the connectivity of pores significantly decrease. As the result, the chloride diffusion coefficient decreases with time [48]. Based on the data from long-term field and laboratory studies, a power law relationship is proposed by Thomas and Bamforth [54], and the function is conmmonly adopted in the later researches [32, 59].

$$D(t) = D_{ref}\left(\frac{t_{ref}}{t}\right)^m \quad (8)$$

where m is the age factor and D_{ref} is the chloride diffusion coefficient at reference time t_{ref} =28 days. However, the defect of this model is that the historic change of the diffusion coefficient for a given exposure duration is not considered, which may lead to an erroneous judgment on chloride ingresses and thus the risk of chloride-induced corrosion [41].

To estimate the crucial parameter m, one can refer to the experimental study conducted by Mangat and Molloy [35]:

$$m = 2.5(W/C) - 0.6 \quad (9)$$

where W/C denotes water cement ratio. It appears that the value of m directly depends on the mix proportion [34], which is represented by W/C. The Eq. (9) is derived by a linear regression analysis with limited data of m and W/C, and the accuracy of predicted relationship can be improved using more data [35].

According to reference [44], the serviceability limit state imposes restrictions on the normal use of a structure, which may involve excessive deformation, vibration, and localized damage such as cracking, spalling, and corrosion. It is widely recognized that when the chloride concentration at the steel location exceeds the chloride threshold level, corrosion of the reinforcement occurs, subsequently leading to cracking and

spalling of the concrete cover. Hence, the LSF for corrosion initiation can be formulated as [68, 69]:

$$G(\mathrm{X},\mathrm{Y}(t),t) = C_{cr} - C(c,t) = C_{cr} - C_s\left[1 - erf\left(\frac{c}{2\sqrt{D(t)t}}\right)\right] \quad (10)$$

where C_{cr} is the chloride threshold level; c represents the depth of the concrete cover over the steel; $C(c, t)$ denotes the concentration of chlorides at depth c and time t.

By considering the LSF as $G(\mathbf{X}, \mathbf{Y}(T_{in}), T_{in})=0$, the time at which corrosion initiation occurs, denoted as T_{in}, can be determined by solving the equation:

$$T_{in} = \left\{\frac{c^2}{4D_{ref}t_{ref}^m}\left[erf^{-1}\left(1 - \frac{C_{cr}}{C_s}\right)\right]^{-2}\right\}^{\frac{1}{1-m}} \quad (11)$$

Since parameters C_{cr}, C_s, c, D_{ref} are all random variables, T_{in} is also a random variable, and the LSF can be rewritten as:

$$G(\mathrm{X},\mathrm{Y}(t),t) = T_{in} - t = \left\{\frac{c^2}{4D_{ref}t_{ref}^m}\left[erf^{-1}\left(1 - \frac{C_{cr}}{C_s}\right)\right]^{-2}\right\}^{\frac{1}{1-m}} - t \quad (12)$$

Utilizing the MCS method, the time-dependent reliability can be computed based on the aforementioned LSF. Notably, the random variable T_{in} and the time parameter t are completely separated in Eq. (12).

By substituting Eq. (12) into Eq. (2), the time-dependent probability of failure can be determined as:

$$\begin{aligned} P_f(0,T) &= Pr(\exists t \in [0,T], T_{in} - t \le 0) \\ &= Pr(\exists t \in [0,T], T_{in} \le t) = F_{T_{in}}(T) \end{aligned} \quad (13)$$

It is evident that the essence of the above formula lies in the cumulative distribution function (CDF) of T_{in}. In other words, the time-dependent probability of failure P_f (0, T) can be evaluated by analyzing $F_{Tin}(T)$.

3. A novel PH fitting method

In view of the limitations inherent in existing reliability analysis methods (such as MCS, FORM, SORM, etc.), it is necessary to address the challenges of accuracy and efficiency. To overcome these challenges, a novel PH fitting method is proposed to accurately and efficiently handle time-dependent reliability problems.

The PH fitting procedure involves estimating the parameters of a PH distribution based on sample data or with respect to another known distribution [55]. The concept of PH distributions was initially introduced by Erlang [16] and later extended by Neuts [37, 38].

PH distributions can be regarded as a generalization of the exponential and Erlang distributions [45]. The representations of PH distributions are depicted in Fig. 1.

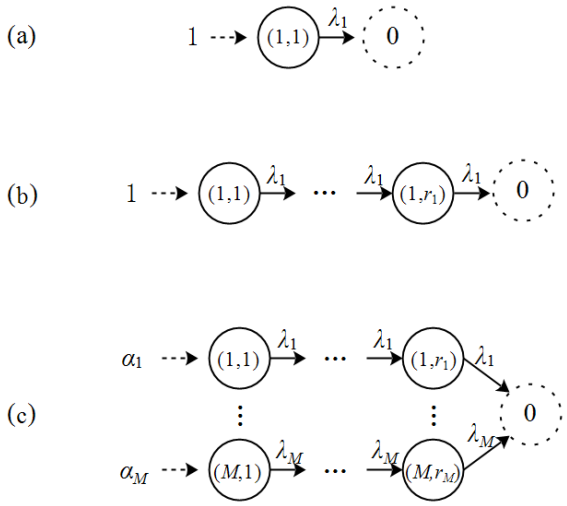

Fig. 1. Representations of PH distributions. (a) Exponential distribution. (b) Erlang distribution. (c) Hyper-Erlang distribution.

As shown in Fig. 1 (a), the exponential distribution is the simplest PH distribution with an order of 1, characterized by a single parameter λ_1. In Fig. 1 (b), the Erlang distribution is featured with two parameters: the rate parameter λ_1 and the shape parameter r_1.

The state transition graph of a hyper-Erlang distribution (HErD) is presented in Fig. 1 (c). The parameters of a HErD include the number of Erlang branches M, the initial probabilities [α_1, α_2, …, α_M], the rate parameters [λ_1, λ_2, …, λ_M], and the shape parameters [r_1, r_2, …, r_M], where $\alpha_1+\alpha_2+\ldots+\alpha_M=1$. Moreover, the order of the HErD, represented by N, is determined by the sum of the shape parameters: $N=r_1+r_2+\ldots+r_M$.

When $M=\alpha_1=1$, the HErD degenerates into the Erlang distribution. Moreover, the exponential distribution is a special case of the HErD with $M=\alpha_1=r_1=1$. Hence, the HErD can be considered as the generalization of the exponential and Erlang distributions. The key of the PH fitting method lies in the determining the parameters of the HErD. Once the relevant parameters are determined, the probability density function (PDF) and CDF of a hyper-Erlang random variable can be expressed as [64]:

$$f(x) = \sum_{m=1}^{M} \alpha_m \frac{(\lambda_m x)^{r_m-1}}{(r_m-1)!}\lambda_m e^{-\lambda_m x} \quad (14)$$

$$F(x) = 1 - \sum_{m=1}^{M} \alpha_m \sum_{i=0}^{r_m-1} \frac{(\lambda_m x)^i}{i!} e^{-\lambda_m x} \quad (15)$$

The steps of the novel PH fitting method are outlined as follows:

1) Initialization

Step 1: Set the initial order as N=1, and initialize the global maximum log-likelihood value as L_{max}= -10^5.

2) Integer splitting method

Step 2: Determine the number of possible branches as M=1, 2, ..., N.

Step 3: Employ the integer splitting method to calculate the number of possible cases of state transition S_N and obtain the corresponding shape parameters $\mathbf{R}_N$: $\{\mathbf{r}_1, \mathbf{r}_2, ..., \boldsymbol{r}_{S_N}\}$.

For instance, if N=4, the possible values for M are 1, 2, ..., 4. Consequently, S_4=5. The partitions of 4 can be represented as {4}, {3, 1}, {2, 2}, {2, 1, 1}, and {1, 1, 1, 1}, as exemplified in Fig. 2.

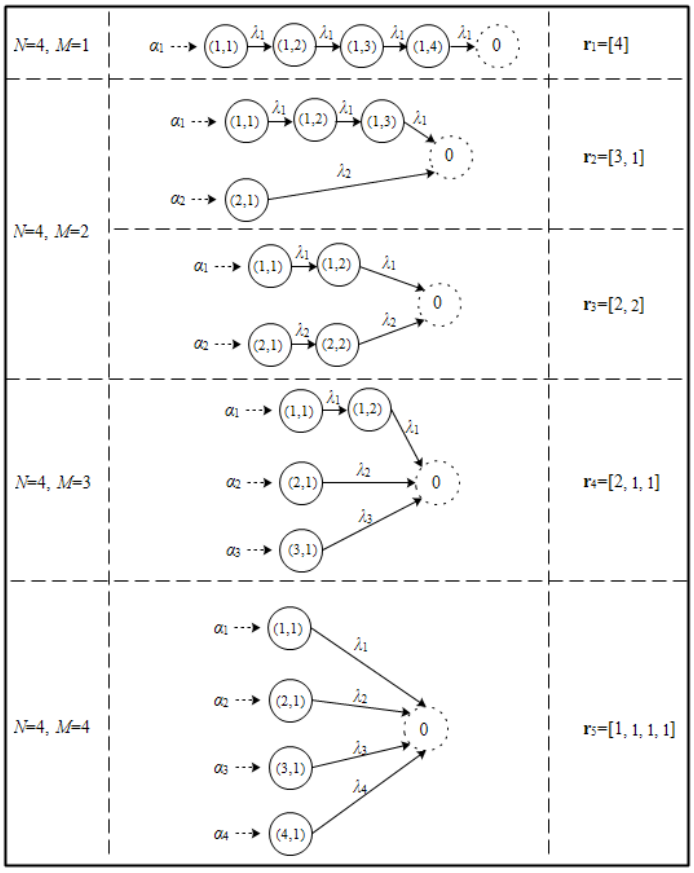

Fig. 2. State transition graphs for N=4, M=1, 2, ..., 4.

3) EM algorithm

The EM algorithm is a valuable tool for estimating parameters from a given data trace [43]. Thus, it is suitable to utilize the EM algorithm to determine the parameters of the HErD. The EM algorithm is executed as follows for a given $\mathbf{r}_n$=[r_1, r_2, …, r_M] (n=1, 2, ..., S_N):

Step 4: Initialize parameters n=1, $\widehat{\boldsymbol{\theta}}_n = (\hat{\alpha}_1, \hat{\alpha}_2, \cdots, \hat{\alpha}_M, \hat{\lambda}_1, \hat{\lambda}_2, \cdots, \hat{\lambda}_M)$.

Step 5: Based on the existing dataset DS={x_1, x_2, ..., x_K}, where K is the number of sample data, compute

$$p_m(x_k|\hat{\lambda}_m) = \hat{\lambda}_m exp[\,(r_m - 1)\, ln(\hat{\lambda}_m x_k) - ln(r_m - 1)! - \hat{\lambda}_m x_k] \quad (16)$$

$$q(m|x_k, \widehat{\boldsymbol{\theta}}_n) = \frac{\hat{\alpha}_m \cdot p_m(x_k|\hat{\lambda}_m)}{\sum_{i=1}^{M} \hat{\alpha}_i \cdot p_i(x_k|\hat{\lambda}_i)} \quad (17)$$

where m=1, 2, ..., M, k=1, 2, ..., K, $ln(r_m - 1)! = \sum_{i=1}^{r_m-1} ln\, i$.

Step 6: Update the parameters using $\boldsymbol{\theta}_n = (\alpha_1, \alpha_2, \cdots, \alpha_M, \lambda_1, \lambda_2, \cdots, \lambda_M)$, expressed as

$$\alpha_m = \frac{1}{K} \sum_{k=1}^{K} q(m|x_k, \widehat{\boldsymbol{\theta}}_n) \quad (18)$$

$$\lambda_m = \frac{r_m \cdot \sum_{k=1}^{K} q(m|x_k, \widehat{\boldsymbol{\theta}}_n)}{\sum_{k=1}^{K} q(m|x_k, \widehat{\boldsymbol{\theta}}_n) \cdot x_k} \quad (19)$$

Step 7: If $max(|\boldsymbol{\theta}_n - \widehat{\boldsymbol{\theta}}_n|) \le \varepsilon = 10^{-6}$, output the parameters $\boldsymbol{\theta}_n$ and go to Step 8; otherwise, set $\widehat{\boldsymbol{\theta}}_n = \boldsymbol{\theta}_n$, and return to Step 5.

Step 8: If $n \le S_N$, set n=n+1, and return to Step 5; otherwise, continue to Step 9.

After repeating Steps 5-8 of the EM algorithm several times, the corresponding output parameters $\boldsymbol{\Theta}_N$: $\{\boldsymbol{\theta}_1, \boldsymbol{\theta}_2, ..., \boldsymbol{\theta}_{S_N}\}$ towards $\mathbf{R}_N$: $\{\mathbf{r}_1, \mathbf{r}_2, ..., \boldsymbol{r}_{S_N}\}$ are got.

Step 9: The log-likelihood values at $\boldsymbol{\theta}_i$ (i=1, 2, ..., S_N) can be calculated as

$$log\, L\,(\boldsymbol{\theta}_i|DS) = log \prod_{k=1}^{K} p(x_k|\boldsymbol{\theta}_i) = \sum_{k=1}^{K} log(\sum_{m=1}^{M} \alpha_m \cdot p_m(x_k|\lambda_m)) = \sum_{k=1}^{K} log(\sum_{m=1}^{M} \alpha_m \cdot \lambda_m\, exp[\,(r_m - 1)\, ln(\lambda_m x_k) - ln(r_m - 1)! - \lambda_m x_k]) \quad (20)$$

And then, the current maximum log-likelihood value L_N, the current optimal output parameters $\boldsymbol{\theta}^*_N$, the optimal index ID, and corresponding optimal $\mathbf{r}^*_N$ can be given by

$$L_N = \max_{1 \le i \le S_N} log\, L\,(\boldsymbol{\theta}_i|DS) \quad (21)$$

$$\boldsymbol{\theta}^*_N = \arg_{\boldsymbol{\theta}} \max_{1 \le i \le S_N} log\, L\,(\boldsymbol{\theta}_i|DS) \quad (22)$$

$$ID = \arg_{i} \max_{1 \le i \le S_N} log\, L\,(\boldsymbol{\theta}_i|DS) \quad (23)$$

$$\mathbf{r}^*_N = \mathbf{r}_{ID} \quad (24)$$

4) Stopping criterion

Step 10: If $L_N \le L_{max}$, set N=N+1, and return to Step 2; otherwise, continue to Step 11.

Step 11: If (L_N - L_{max})/$|L_{max}| \le \delta = 10^{-3}$, the algorithm

terminates and output the global optimal parameters $\boldsymbol{\theta}^*=\boldsymbol{\theta}^*_N$, $\mathbf{r}^*=\mathbf{r}^*_N$; otherwise, set $L_{\max}=L_N$, $N=N+1$, and return to Step 2.

The flowchart of the PH fitting method is shown in Fig. 3.

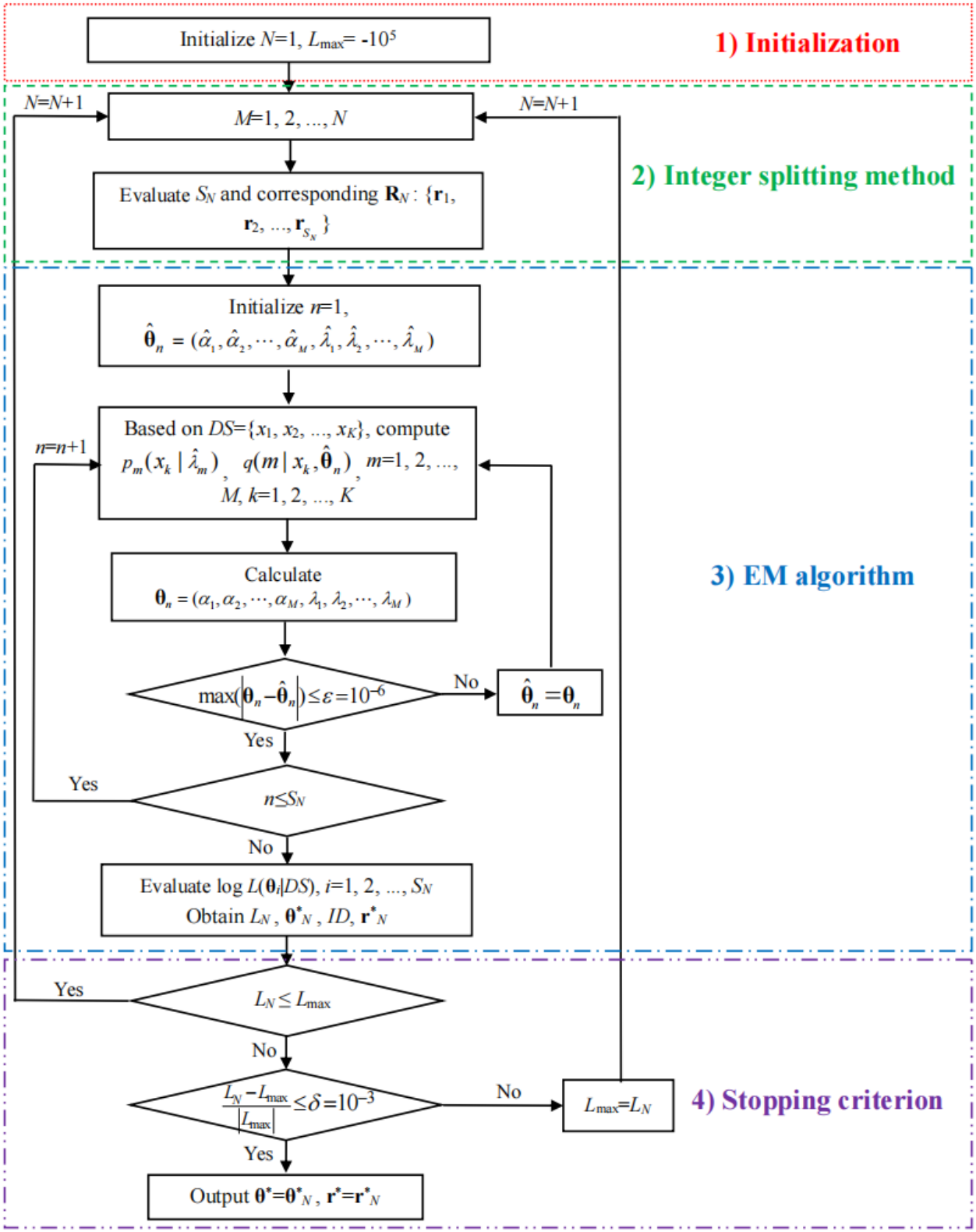

Fig. 3. Flowchart of the PH fitting method.

4. Illustrative examples

In the field of reliability, conventional distributions commonly used include the lognormal, normal, gamma, exponential, Weibull, and type I extreme value (also known as the Gumbel) distributions [6, 21, 25, 27, 28, 30, 39, 49, 51, 52]. In this section, these six typical distributions are employed to validate the effectiveness of the novel PH fitting method. Additionally,

the proposed method is applied to an example involving corroded RC beams.

4.1. Numerical examples

In the first example, four datasets with sample sizes of K=50, 250, 500 and 10^4 are generated from the lognormal distribution, where the mean value is μ=2 and the standard deviation is σ=1. The iterative process of the PH fitting method for this example is presented in detail in Table 1.

Table 1. Iterative process of the PH fitting method for the lognormal distribution dataset.

Lognormal distribution dataset with K=50									
N	S_N	$L_{\max}$	L_N	$\frac{L_N - L_{max}}{\lvert L_{max} \rvert \lvert \lvert}$	ID	$\mathbf{r}^*_N$	$\boldsymbol{\theta}^*_N$		M
							$\boldsymbol{\alpha}^*_N$	$\boldsymbol{\lambda}^*_N$	
1	1	-10^5	-81.492	0.9992	1	[1]	[1]	[0.5327]	1
2	2	-81.492	-67.2944	0.1742	1	[2]	[1]	[1.0654]	1
3	3	-67.2944	-61.5918	0.0847	1	[3]	[1]	[1.5980]	1
4	5	-61.5918	-59.1726	0.0393	1	[4]	[1]	[2.1307]	1
5	7	-59.1726	-58.5038	0.0113	1	[5]	[1]	[2.6634]	1
6	11	-58.5038	-58.475	0.0005	2	[5, 1]	[0.9876, 0.0124]	[2.6900, 0.2974]	2
Lognormal distribution dataset with K=250									
N	S_N	$L_{\max}$	L_N	$\frac{L_N - L_{max}}{\lvert L_{max} \rvert \lvert \lvert}$	ID	$\mathbf{r}^*_N$	$\boldsymbol{\theta}^*_N$		M
							$\boldsymbol{\alpha}^*_N$	$\boldsymbol{\lambda}^*_N$	
1	1	-10^5	-414.1856	0.9959	1	[1]	[1]	[0.5185]	1
2	2	-414.1856	-347.3264	0.1614	1	[2]	[1]	[1.0371]	1
3	3	-347.3264	-322.9418	0.0702	1	[3]	[1]	[1.5556]	1
4	5	-322.9418	-314.974	0.0247	1	[4]	[1]	[2.0742]	1
5	7	-314.974	-313.8942	0.0034	2	[4, 1]	[0.9863, 0.0137]	[2.1124,0.2253]	2
6	11	-313.8942	-311.8361	0.0066	2	[5, 1]	[0.9695, 0.0305]	[2.6790, 0.2562]	2
7	15	-311.8361	-310.0493	0.0057	3	[5, 2]	[0.9345, 0.0655]	[2.7353, 0.5946]	2
8	22	-310.0493	-309.312	0.0024	4	[5, 3]	[0.9127, 0.0873]	[2.7819, 0.9094]	2
9	30	-309.312	-309.312	-	-	-	-	-	-
10	42	-309.312	-308.7658	0.0018	9	[6, 3, 1]	[0.8271, 0.1729, 0.0000]	[3.4580, 1.0513, 0.3417]	3
11	56	-308.7658	-308.3769	0.0013	10	[6, 4, 1]	[0.8195, 0.1805, 0.0000]	[3.5275, 1.3506, 0.3129]	3
12	77	-308.3769	-308.3653	3.762×10^{-5}	12	[6, 5, 1]	[0.8487, 0.1513, 0.0000]	[3.5301, 1.5565, 0.3005]	3
Lognormal distribution dataset with K=500									
N	S_N	$L_{\max}$	L_N	$\frac{L_N - L_{max}}{\lvert L_{max} \rvert \lvert \lvert}$	ID	$\mathbf{r}^*_N$	$\boldsymbol{\theta}^*_N$		M
							$\boldsymbol{\alpha}^*_N$	$\boldsymbol{\lambda}^*_N$	
1	1	-10^5	-840.2996	0.9916	1	[1]	[1]	[0.5063]	1
2	2	-840.2996	-703.9033	0.1623	1	[2]	[1]	[1.0126]	1
3	3	-703.9033	-652.4565	0.0731	1	[3]	[1]	[1.5189]	1
4	5	-652.4565	-633.8432	0.0285	1	[4]	[1]	[2.0253]	1
5	7	-633.8432	-632.7352	0.0017	1	[5]	[1]	[2.5316]	1
6	11	-632.7352	-628.396	0.0069	2	[5, 1]	[0.9723, 0.0277]	[2.6006, 0.2622]	2
7	15	-628.396	-624.9534	0.0055	3	[5, 2]	[0.9368, 0.0632]	[2.6555, 0.5986]	2

8	22	-624.9534	-623.3381	0.0026	4	[5, 3]	[0.9112, 0.0888]	[2.7019, 0.9224]	2
9	30	-623.3381	-620.94	0.0038	4	[6, 3]	[0.8321, 0.1679]	[3.3490, 1.0402]	2
10	42	-620.94	-620.94	-	-	-	-	-	-
11	56	-620.94	-619.9419	0.0016	10	[6, 4, 1]	[0.8145, 0.1855, 0.0000]	[3.4244, 1.3542, 0.3639]	3
12	77	-619.9419	-619.4968	0.0007	11	[7, 4, 1]	[0.6886, 0.3114, 0.0000]	[4.1880, 1.5114, 0.3563]	3

Lognormal distribution dataset with K=10^4

N	S_N	$L_{\max}$	L_N	$\frac{L_N - L_{max}}{\|L_{max}\|\|}$	ID	$\mathbf{r}^*_N$	$\boldsymbol{\theta}^*_N$		M
							$\boldsymbol{\alpha}^*_N$	$\boldsymbol{\lambda}^*_N$	
1	1	-10^5	-16927	0.8307	1	[1]	[1]	[0.5002]	1
2	2	-16927	-14168	0.163	1	[2]	[1]	[1.0004]	1
3	3	-14168	-13108	0.0748	1	[3]	[1]	[1.5006]	1
4	5	-13108	-12705	0.0307	1	[4]	[1]	[2.0008]	1
5	7	-12705	-12651	0.0043	1	[5]	[1]	[2.5010]	1
6	11	-12651	-12585	0.0052	2	[5, 1]	[0.9829, 0.0171]	[2.5464, 0.2471]	2
7	15	-12585	-12540	0.0036	3	[5, 2]	[0.9552, 0.0448]	[2.5884, 0.5816]	2
8	22	-12540	-12517	0.0018	4	[5, 3]	[0.9289, 0.0711]	[2.6303, 0.9137]	2
9	30	-12517	-12479	0.003	4	[6, 3]	[0.8406, 0.1594]	[3.2687, 1.0482]	2
10	42	-12479	-12479	-	-	-	-	-	-
11	56	-12479	-12457	0.0018	10	[6, 4, 1]	[0.8112, 0.1888, 0.0000]	[3.3508, 1.3817, 0.3036]	3
12	77	-12457	-12451	0.0005	11	[7, 4, 1]	[0.6836, 0.3164, 0.0000]	[4.0861, 1.5284, 0.2624]	3

For the dataset with the sample size K=50, after 6 iterations, it is apparent that the global optimal parameters are identified as $\mathbf{r}^*$=[5, 1], $\boldsymbol{\alpha}^*$=[0.9876, 0.0124], $\boldsymbol{\lambda}^*$=[2.6900, 0.2974]. And after 12 iterations, the optimal parameters are obtained as $\mathbf{r}^*$=[6, 5, 1], $\boldsymbol{\alpha}^*$=[0.8487, 0.1513, 0.0000], $\boldsymbol{\lambda}^*$=[3.5301, 1.5565, 0.3005] for K=250.

Regardless of whether the sample size K is 500 or 10^4, it is evident from the provided table that the maximum log-likelihood value L_N for N=10 (i.e., L_{10}) satisfies the condition $L_{10} \leq L_{\max}$. This implies that L_{10} does not contribute to the improvement of $L_{\max}$. Therefore, this iteration (N=10) is considered invalid, and the next iteration (N=11) is necessary.

After 12 iterations, the iterative process terminates and the global optimal parameters are determined as $\mathbf{r}^*$=[7, 4, 1], $\boldsymbol{\alpha}^*$=[0.6886, 0.3114, 0.0000], $\boldsymbol{\lambda}^*$=[4.1880, 1.5114, 0.3563] for K=500, and $\mathbf{r}^*$=[7, 4, 1], $\boldsymbol{\alpha}^*$=[0.6836, 0.3164, 0.0000], $\boldsymbol{\lambda}^*$=[4.0861, 1.5284, 0.2624] for K=10^4. Once the optimal parameters of the HErD are obtained, the PDF and CDF can be derived using Eqs. (14) and (15).

The empirical PDF (i.e., the outer contour of the frequency histogram), the PDF obtained through kernel density estimation, as well as the PDF resulting from Gaussian fitting and PH fitting, are compared with the PDF of the lognormal distribution with μ=2 and σ=1. The results are presented in Fig.4

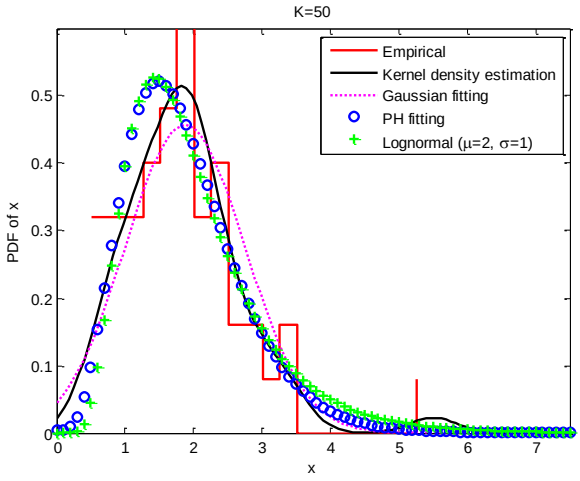

a)

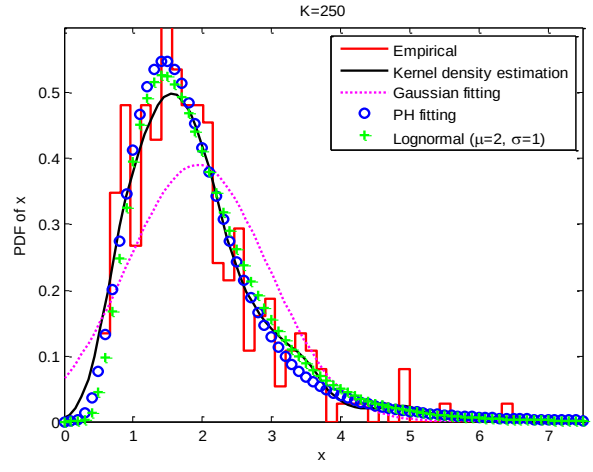

b)

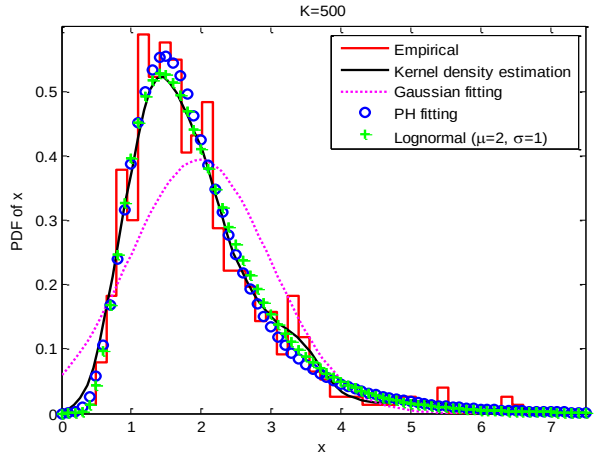

c)

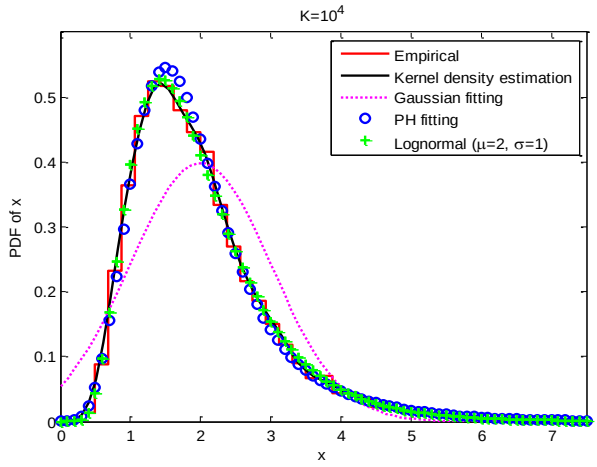

d)

Fig. 4. Comparison of the fitting results for the lognormal distribution dataset. (a) K=50. (b) K=250. (c) K=500. (d) K=10^4.

Furthermore, the PH fitting results with different sample sizes of K=50, 250, 500, 10^4 and the true PDF of the lognormal distribution are plotted in Fig. 5.

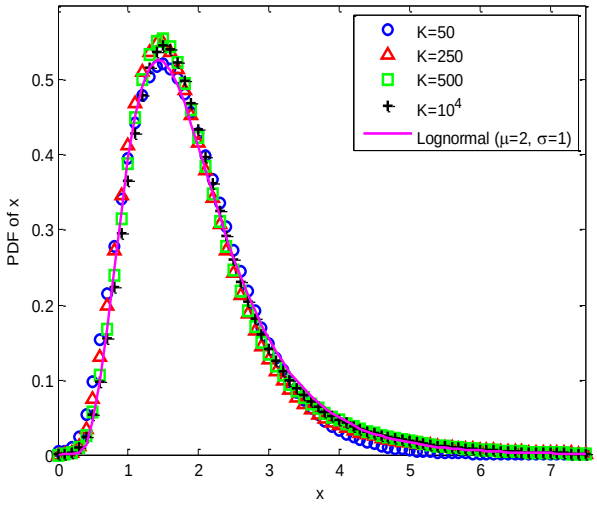

Fig. 5. Comparison of the fitting results with different sample sizes.

It can be seen from Fig. 5 that the fitting results for different sample sizes of K=50, 250, 500 and 10^4 are all close to the true PDF of the lognormal distribution, showing the accuracy and robustness of the PH fitting method towards the data with different sample sizes.

The other five distributions will be discussed next. A dataset with sample size of K=500 is generated from the normal distribution, where the mean value is μ=3 and the standard deviation is σ=1. And another dataset with the same sample size is generated from the gamma distribution with shape parameter A=0.4 and scale parameter B=0.25. The datasets from the exponential distribution with mean value μ=5, the weibull distribution with shape parameter A=3 and scale parameter B=3, and the type I extreme value (or gumbel) distribution with mean value μ=2 and standard deviation σ=1 are also investigated. The optimal parameters for distribution datasets and the fitting results are displayed in Table 2 and Fig. 6, respectively.

Table 2. The optimal parameters for different distribution datasets with K=500.

Distribution dataset with K=500										
Distribution	N	S_N	$L_{\max}$	L_N	$\frac{L_N - L_{\max}}{\lvert L_{\max} \rvert}$	ID	$\mathbf{r}^*_N$	$\boldsymbol{\theta}^*_N$		M
								$\boldsymbol{\alpha}^*_N$	$\boldsymbol{\lambda}^*_N$	
Normal	18	385	-695.4227	-694.8141	0.0009	5	[14, 4]	[0.8561, 0.1439]	[4.3271, 2.0465]	2
Gamma	18	385	936.322	936.7508	0.0005	167	[7, 4, 3, 2, 1, 1]	[0.1727, 0.2061, 0.1601, 0.3724, 0.0443, 0.0443]	[177, 305, 1626, 9, 10543, 10543]	6
Exponential	3	3	-1302.8	-1302.5	0.0002	2	[2, 1]	[0.3995, 0.6005]	[0.2428, 0.3554]	2
Weibull	17	297	-676.7212	-676.0782	0.0010	6	[12, 5]	[0.7387, 0.2613]	[4.0582, 2.5307]	2
Type I extreme value (or Gumbel)	9	30	-651.2021	-651.1546	0.0001	4	[6, 3]	[0.6282, 0.3718]	[3.0368, 1.4339]	2

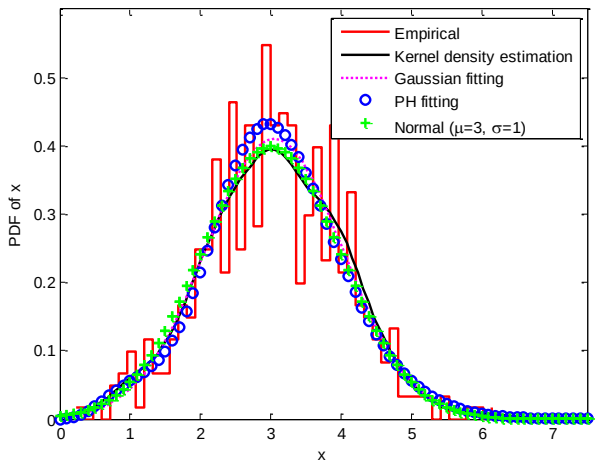

a)

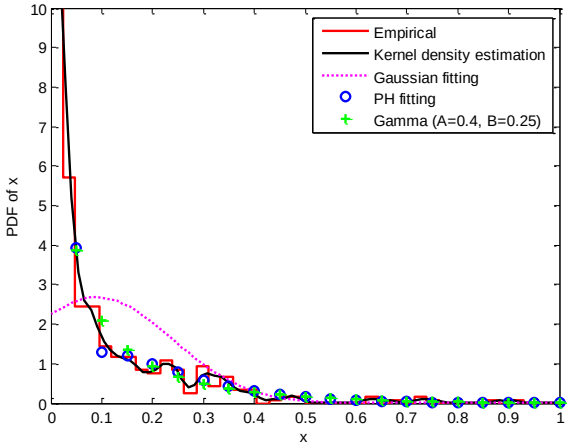

b)

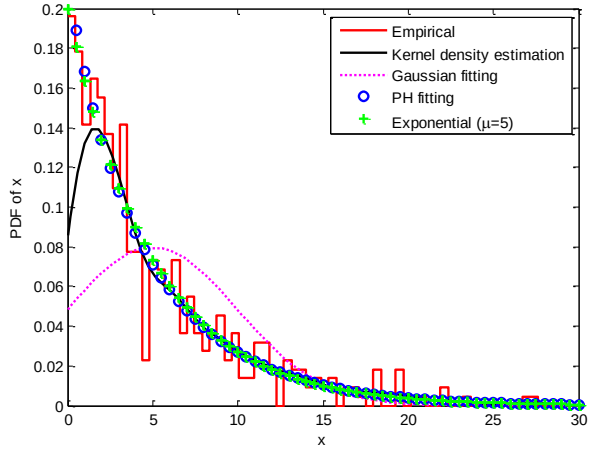

c)

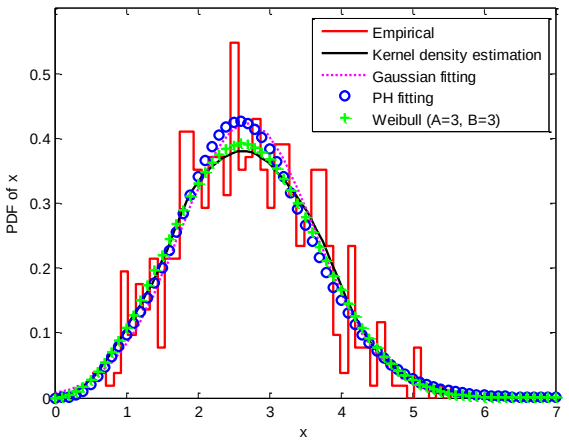

d)

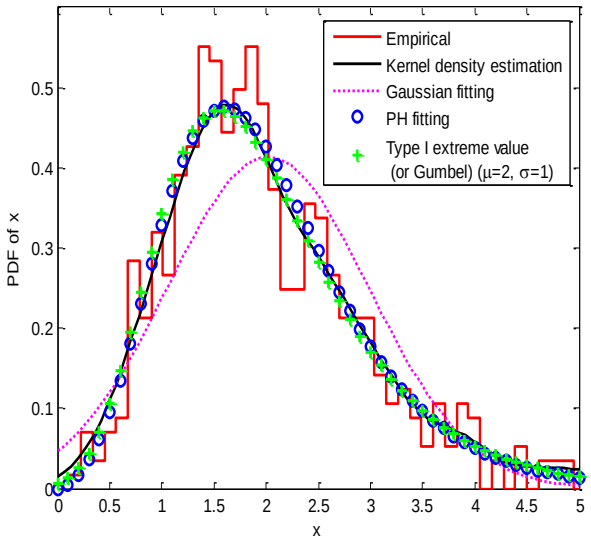

e)

Fig. 6. Comparison of the fitting results for different distribution datasets with K=500. (a) Normal. (b) Gamma. (c) Exponential. (d) Weibull. (e) Type I extreme value (or Gumbel).

It can been seen from Fig. 5 that the PDF obtained by different methods are close enough, indicating the effectiveness of the PH fitting method.

4.2. An example of time-dependent reliability analysis of corroded RC beams

To further illustrate the application of the PH fitting method, an example involving corroded RC beams is presented. The LSF for this example focuses on the corrosion initiation of the reinforced steel. The parameters utilized in the example are derived from relevant literature [15, 47, 60, 70] and are summarized in Table 3.

Table 3. Distribution of random parameters for the corroded RC beams.

Parameter	Distribution	Mean	Coefficient of variation	Source
C_{cr}	Uniform	0.9 kg/m^3	0.2	[15]
C_s	Lognormal	3.5 kg/m^3	0.2	[70]
c	Normal	30 mm	0.2	[60]
D_{ref}	Lognormal	12×10^{-12} m^2/s	0.2	[47]

As indicated in Eq. (9), the age factor m is determined by the water cement ratio (W/C). In this particular example, the value of W/C is selected as 0.35, 0.4, or 0.45. Consequently, the corresponding values of m are calculated using Eq. (9) as 0.275, 0.4, or 0.525, respectively. Assuming $D_{ref}=12\times10^{-12}$ m^2/s, the relationships between the chloride diffusion coefficient $D(t)$ and time t are plotted in Fig. 7.

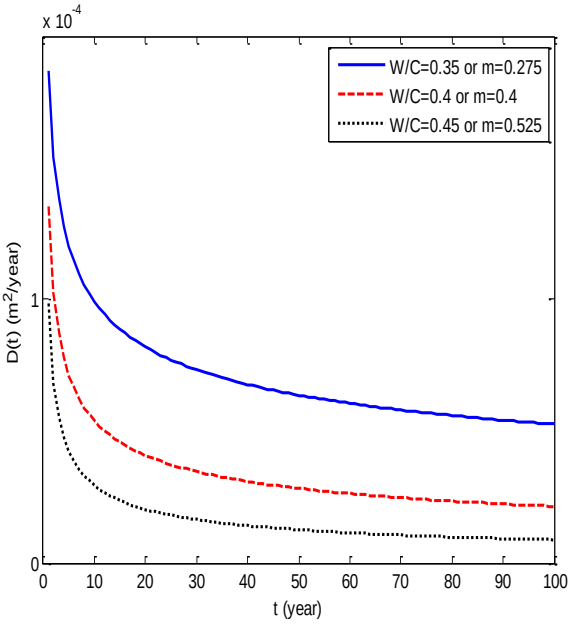

Fig. 7. The variation of $D(t)$.

It is illustrated that $D(t)$ exhibits a rapid decrease during the early stages and a slower decline in the later period. To ensure that $D(t)$ decreases with t [61], it is necessary to limit the value of m within the range of 0 to 1. Gjorv [19] suggested setting m to 0.4, a value consistent with the empirical formula [34]. Therefore, m=0.4 (corresponding to W/C=0.4) is adopted in this study. Subsequently, the LSF in Eq. (12) can be expressed as follows:

$$G(X,Y(t),t)=T_{in}-t=\left\{\frac{c^2}{4D_{ref}\left(\frac{28}{365}\right)^{0.4}}\left[erf^{-1}\left(1-\frac{C_{cr}}{C_s}\right)\right]^{-2}\right\}^{\frac{1}{1-0.4}}-t \quad (25)$$

where t represents the time parameter varying within [0, 100] years, $\mathbf{X}=[C_{cr}, C_s, c, D_{ref}]^{\mathrm{T}}$ denotes the random variables. Since $\mathbf{Y}(t)$ does not appear in this case, one can obtain $\mathbf{W}=[\mathbf{X}, \mathbf{Y}(t)]=[\mathbf{X}, \mathbf{Z}]=[C_{cr}, C_s, c, D_{ref}]^{\mathrm{T}}$. Both the PH fitting method described in Section 3 and the MCS method are employed to calculate the time-dependent reliability.

In the PH fitting method, 500 random samples of $\mathbf{W}$ are initially generated according to their respective distributions. Based on these random samples, 500 corrosion initiation times T_{in} can be computed using Eq. (25). The PDF of T_{in} is then approximated using kernel density estimation, Gaussian fitting, and PH fitting methods. These approximations are compared

with the empirical PDF, and the results are presented in Fig. 8.

Figure 8 clearly demonstrates that the corrosion initiation time T_{in} can be effectively approximated using the PH fitting method. The reason why the PH fitting method outperforms other methods is that the PH method can make full use of the positive dataset, accurately capture its distribution characteristics and efficiently estimate relevant parameters. Directly approximating to some conventional distributions may ignore the features of the dataset, and result in significant errors. The iterative process to obtain the optimal parameters for the PH fitting method is outlined in Table 4.

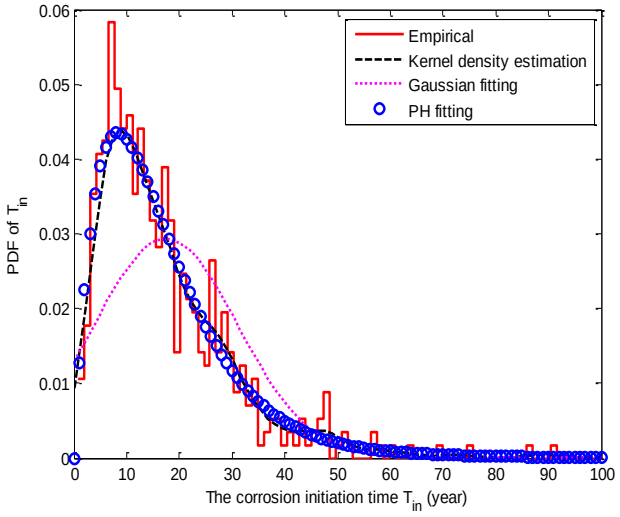

Fig. 8. Comparison of different approximation methods for PDF.

Table 4. Iterative process of corroded RC beams.

N	S_N	$L_{\max}$	L_N	$\frac{L_N - L_{\max}}{\lvert L_{\max}\rvert}$	ID	$\mathbf{r}^*_N$	$\boldsymbol{\theta}^*_N$		M
							$\boldsymbol{\alpha}^*_N$	$\boldsymbol{\lambda}^*_N$	
1	1	-10^5	-1930	0.9807	1	[1]	[1]	[0.0573]	1
2	2	-1930	-1869.2	0.0315	1	[2]	[1]	[0.1145]	1
3	3	-1869.2	-1866.4	0.0015	2	[2, 1]	[0.9716, 0.0284]	[0.1191, 0.0246]	2
4	5	-1866.4	-1866.4	-	-	-	-	-	-
5	7	-1866.4	-1865.4	0.0005	3	[3, 2]	[0.0302, 0.9698]	[0.0595, 0.1217]	2

After 5 iterations, the iterative process of the PH fitting method concludes, and the optimal parameters are determined as $\mathbf{r}^*$=[3, 2], $\boldsymbol{\alpha}^*$=[0.0302, 0.9698], and $\boldsymbol{\lambda}^*$=[0.0595, 0.1217]. With these optimal parameters, the CDF of T_{in} can be calculated using Eq. (15). According to Eq. (13), it is known that the time-dependent probability of failure $P_f(0, t)$ ($t \in [0, 100]$ years) can be evaluated through the CDF of T_{in}, i.e., $F_{Tin}(t)$.

In the MCS [7, 67] method, the time interval is discretized with Δt set as 1 year, resulting in a total of s=101 time nodes. 10^5 MCS samples of $\mathbf{W}$ are generated, and the corresponding values of the LSF are computed at each time node. Therefore, the MCS method requires $N_{\text{call}}=101\times10^5$ function calls in total. For the t-IRS [30] method, 30 initial samples are first generated to construct an initial instantaneous response surrogate model. And extra 54 samples are then selected to update the surrogate model. The comparison results of the three different methods are presented in Fig. 9 and Table 5.

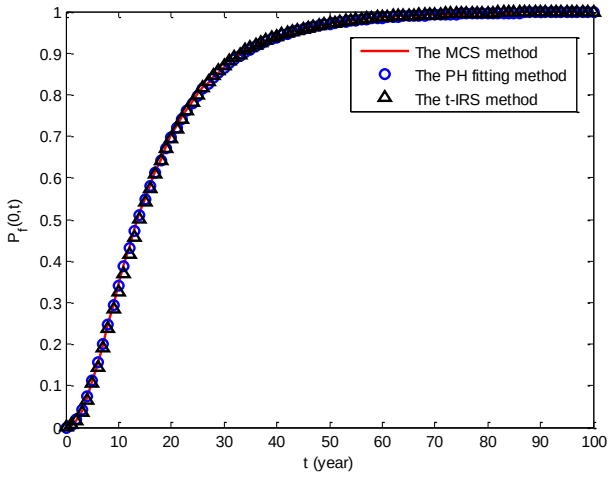

Fig. 9. Comparison of the MCS, PH fitting and t-IRS methods.

Table 5. Failure probability results for the MCS, PH fitting and t-IRS methods.

Time interval	MCS [23, 24]	PH fitting		t-IRS [54]	
		P_f	Error (%)	P_f	Error (%)
[0, 10]	0.3471	0.3338	3.8317	0.3193	8.0092
[0, 20]	0.7020	0.6814	2.9345	0.6794	3.2194
[0, 30]	0.8665	0.8607	0.6694	0.8757	1.0617
[0, 40]	0.9396	0.9389	0.0745	0.9419	0.2448
[0, 50]	0.9709	0.9714	0.0515	0.9724	0.1545
[0, 60]	0.9859	0.9853	0.0609	0.9873	0.1420
[0, 70]	0.9921	0.9917	0.0403	0.9935	0.1411
[0, 80]	0.9960	0.9950	0.1004	0.9973	0.1305
[0, 90]	0.9977	0.9968	0.0902	0.9989	0.1203
[0, 100]	0.9988	0.9980	0.0801	0.9999	0.1101
N_{call}	101×10^5	500	-	30+54	-

As mentioned previously, the MCS method is so accurate that the result is often taken as the reference one. The efficiency and accuracy of the PH fitting method are compared in terms of N_{call} and Error (%).

In terms of computational efficiency, it can be seen from Table 5 that the MCS method requires 101×10^5 function calls to obtain the reliability. In comparison, the proposed PH fitting method only necessitates 500 function calls, showing its efficiency in reducing the computational burden significantly. Furthermore, when considering the reliability accuracy, the errors of the PH fitting method for all time intervals are consistently below 5%, and in some cases, even below 0.1%. This demonstrates that the PH fitting method maintains the accuracy of reliability assessment. Compared with the MCS method, it can be concluded that the PH fitting method achieves a remarkable reduction in computational burden while ensuring the reliability accuracy.

However, the efficiency of the proposed method is lower than that of t-IRS, but its accuracy is always better than t-IRS. The PH fitting method is a universal method for solving reliability problems with positive dataset. For more complex structural systems, the proposed method is required to incorporate with other system reliability strategies.

Furthermore, the sensitivity analysis of the mean for different parameters (C_{cr}, C_s, c and D_{ref}) are investigated. The corresponding reliability results with different means are displayed in Fig. 10.

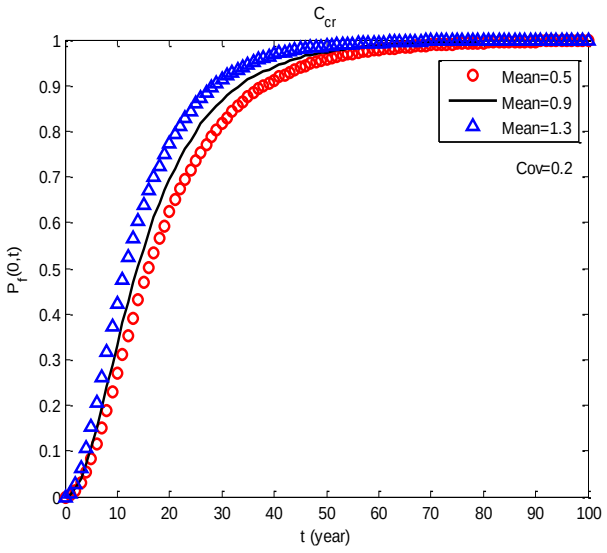

a)

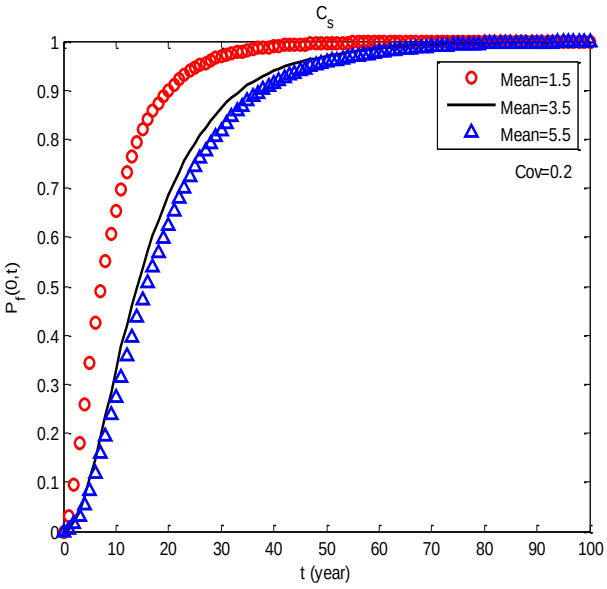

b)

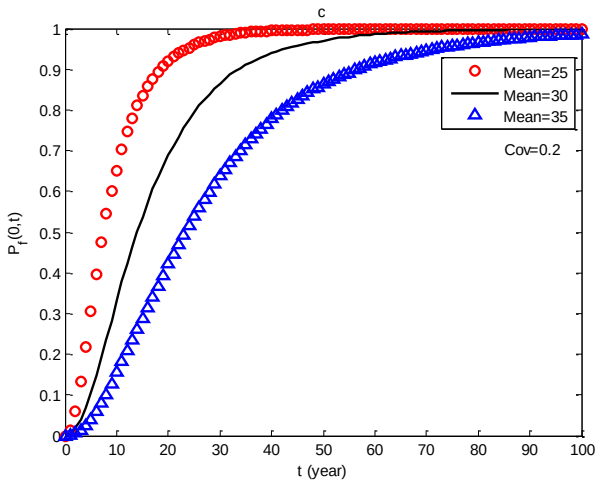

c)

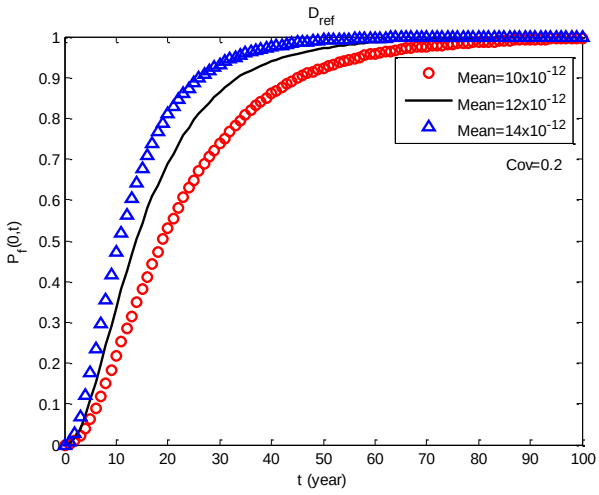

d)

Fig. 10. Failure probability results with different means. (a) C_{cr}. (b) C_s. (c) c. (d) D_{ref}.

It can be seen from the sensitivity analysis that the means of random parameters have great effects on the final reliability results. With the increase of C_{cr} and D_{ref} or the decrease of C_s and c, the failure probability of the RC structure will increase. Therefore, it is vital to accurately determine relevant statistical information of parameters and quantitatively define the parameter uncertainties.

5. Conclusions

This paper studies the time-dependent reliability analysis of corroded RC beams based on the PH fitting method. A reliability model of RC structures is first formulated by taking the time-dependent chloride diffusion coefficient into consideration. Next, a new strategy is cooperated with EM algorithm to simply, efficiently and scientifically obtain the parameters of PH fitting method. The effectiveness of the new method is then demonstrated using several numerical examples. Finally, the novel PH fitting method is applied to an example of corroded RC beams. The proposed method is shown to be an useful way in calculating the time-dependent reliability, and the results show excellent computational efficiency and accuracy compared with the MCS method.

The main contributions of this paper are threefold: 1) formulating a reliability model of RC structures by taking into account the time-dependent chloride diffusion coefficient; 2) a new strategy is utilized to simply, efficiently and scientifically obtain the parameters of PH fitting method; 3) using the novel PH fitting method to accurately and efficiently deal with time-dependent reliability analysis of corroded RC beams.

The new method is limited to the property of PH distribution that only the positive support can be approximated as the PH distribution. In other words, the PH distribution is inapplicable to approximate the dataset with negative numbers.

Further studies will include: 1) considering the corrosion model for concrete; 2) taking into account the correlations between random variables; 3) applying the new method to more complex civil engineering problems; 4) integrating the proposed method with different optimization algorithms to optimize practical engineering problems.

Acknowledgement

This work is supported by the National Natural Science Foundation of China (nos. 52275266, 11832013 and 11572134), Hubei Provincial Department of Education Science and Technology Research Project (no. Q20221714), and the Opening Foundation of Hubei Key Laboratory of Digital Textile Equipment (no. DTL2022012). The authors sincerely thank the editor and anonymous reviewers for the constructive comments on this paper.

References

1. Alkaff A, Qomarudin M N, Bilfaqih Y. Network reliability analysis: Matrix-exponential approach. Reliability Engineering and System Safety 2020; 204: 107192. https://doi.org/10.1016/j.ress.2020.107192

2. Amey S L, Johnson D A, Miltenberger M A, Farzam H. Predicting the service life of concrete marine structures: an environmental methodology. ACI Structural Journal 1998; 95(2): 205-214. https://doi.org/10.14359/540
3. Awad M, Senga Kiesse T, Assaghir Z, Ventura A. Convergence of sensitivity analysis methods for evaluating combined influences of model inputs. Reliability Engineering and System Safety 2019; 189: 109-122. https://doi.org/10.1016/j.ress.2019.03.050
4. Bader M A. Performance of concrete in a coastal environment. Cement and Concrete Composites 2003; 25: 539-548. https://doi.org/10.1016/S0958-9465(02)00093-8
5. Bagheri M, Abbas Hosseini S, Keshtegar B, Correia J A F O, Trung N T. Uncertain time-dependent reliability analysis of corroded RC structures applying three-term conjugate method. Engineering Failure Analysis 2020; 115: 104599. https://doi.org/10.1016/j.engfailanal.2020.104599
6. Balakrishnan N, So H Y, Ling M H. EM algorithm for one-shot device testing with competing risks under exponential distribution. Reliability Engineering and System Safety 2015; 137: 129-140. https://doi.org/10.1016/j.ress.2014.12.014
7. Betz W, Papaioannou I, Straub D. Bayesian post-processing of Monte Carlo simulation in reliability analysis. Reliability Engineering and System Safety 2022; 227: 108731. https://doi.org/10.1016/j.ress.2022.108731
8. Chen J, Qian C. Loading history dependence of retardation time of calcium-silicate-hydrate. Construction and Building Materials 2017; 147: 558-565. https://doi.org/10.1016/j.conbuildmat.2017.04.183
9. Chen S, Lu L, Xiang Y, Lu Q, Li M. A data heterogeneity modeling and quantification approach for field pre-assessment of chloride-induced corrosion in aging infrastructures. Reliability Engineering and System Safety 2018; 171: 123-135. https://doi.org/10.1016/j.ress.2017.11.013
10. Collepardi M, Marcialis A, Turriziani R. Penetration of chloride ions into cement pastes and concretes. Journal of the American Ceramic Society 1972; 55(10): 534-535. https://doi.org/10.1111/j.1151-2916.1972.tb13424.x
11. Crank J. The mathematics of diffusion, 2nd ed. London: Oxford University Press, 1975.
12. Dembińska A, Eryilmaz S. Discrete time series-parallel system and its optimal configuration. Reliability Engineering and System Safety 2021; 215: 107832. https://doi.org/10.1016/j.ress.2021.107832
13. Ding H, Chen J. Research on the resistivity attenuation law of cementitious conductive composites induced by stress relaxation. Construction and Building Materials 2019; 206: 347-354. https://doi.org/10.1016/j.conbuildmat.2019.02.075
14. El Hajj Chehade F, Younes R, Mroueh H, Hage Chehade F. Time-dependent reliability analysis for a set of RC T-beam bridges under realistic traffic considering creep and shrinkage. European Journal of Environmental and Civil Engineering 2022; 26(13): 6480-6504. https://doi.org/10.1080/19648189.2021.1946720
15. El Hassan J, Bressolette P, Chateauneuf A, El Tawil K. Reliability-based assessment of the effect of climatic conditions on the corrosion of RC structures subject to chloride ingress. Engineering Structures 2010; 32(10): 3279-3287. https://doi.org/10.1016/j.engstruct.2010.07.001
16. Erlang A K. Solution of some problems in the theory of probabilities of significance in automatic telephone exchanges. Post Office Electrical Engineer's Journal, 1917; 10: 189-197.
17. Fan X, Zhou H, Liu Y. Time-Dependent Reliability Analysis of RC Bridges Considering Shrinkage, Creep, Resistance Degradation, and Vehicle Load Flows. Advances in Civil Engineering 2023; 2023: 5111719. https://doi.org/10.1155/2023/5111719
18. Francesco D M, Matteo F, Carlo G, Federico P, Enrico Z. Time-dependent reliability analysis of the reactor building of a nuclear power plant for accounting of its aging and degradation. Reliability Engineering and System Safety 2021; 205: 107173. https://doi.org/10.1016/j.ress.2020.107173
19. Gjorv O E. Durability of concrete structures. Arabian Journal for Science and Engineering 2011; 36(2): 151-172. https://doi.org/10.1007/s13369-010-0033-5
20. Guo H, Jiang C, Gu X, Dong Y, Zhang W. Time-dependent reliability analysis of reinforced concrete beams considering marine environmental actions. Engineering Structures 2023; 288: 116252. https://doi.org/10.1016/j.engstruct.2023.116252
21. Hong H P. Selection of regressand for fitting the extreme value distributions using the ordinary, weighted and generalized least-squares methods. Reliability Engineering and System Safety 2013; 118: 71-80. https://doi.org/10.1016/j.ress.2013.04.003
22. Hong N. Corrosion and protective technology of rebar in concrete (3): Rebar corrosion by chloric salt. Industrial Construction 1999;

29(10) :60-63.

23. Kassir M K, Ghosn M. Chloride-induced corrosion of reinforced concrete bridge decks. Cement and Concrete Research 2002; 32(1): 139-143. https://doi.org/10.1016/S0008-8846(01)00644-5
24. Kim J, McCarter W J, Suryanto B, Nanukuttan S, Basheer P A M, Chrisp T M. Chloride ingress into marine exposed concrete: A comparison of empirical- and physically- based models. Cement and Concrete Composites 2016; 72: 133-145. https://doi.org/10.1016/j.cemconcomp.2016.06.002
25. Li J, Chen J. Solving time-variant reliability-based design optimization by PSO-t-IRS: A methodology incorporating a particle swarm optimization algorithm and an enhanced instantaneous response surface. Reliability Engineering and System Safety 2019; 191: 106580. https://doi.org/10.1016/j.ress.2019.106580
26. Li J, Chen J, Chen Z. Developing an improved composite limit state method for time-dependent reliability analysis. Quality Engineering 2020; 32(3): 298-311. https://doi.org/10.1080/08982112.2020.1735004
27. Li J, Chen J, Chen Z. A new cumulative damage model for time-dependent reliability analysis of deteriorating structures. Proceedings of the Institution of Mechanical Engineers, Part O: Journal of Risk and Reliability 2020; 234(2): 290-302. https://doi.org/10.1177/1748006X19886157
28. Li J, Chen J, Wei J, Yang X. Temporal-spatial reliability analysis of RC bridges with corroded steel reinforcement bars. Proceedings of the Institution of Mechanical Engineers, Part C: Journal of Mechanical Engineering Science 2022; 236(23): 11345-11357. https://doi.org/10.1177/09544062221105985
29. Li J, Chen J, Wei J, Yang X. A Kriging-based important region sampling method for efficient reliability analysis. Quality Technology and Quantitative Management 2023; 20(3): 360-383. https://doi.org/10.1080/16843703.2022.2116265
30. Li J, Chen J, Wei J, Zhang X, Han B. Developing an instantaneous response surface method t-IRS for time-dependent reliability analysis. Acta Mechanica Solida Sinica 2019; 32(4): 446-462. https://doi.org/10.1007/s10338-019-00096-5
31. Li J, Chen J, Zhang X. Time-dependent reliability analysis of deteriorating structures based on Phase-type distributions. IEEE Transactions on Reliability 2020; 69(2): 545-557. https://doi.org/10.1109/TR.2019.2907307
32. Li Q, Ye X. Surface deterioration analysis for probabilistic durability design of RC structures in marine environment. Structural Safety 2018; 75: 13-23. https://doi.org/10.1016/j.strusafe.2018.05.007
33. Liu B, Wen Y, Qiu Q, Shi H, Chen J. Reliability analysis for multi-state systems under K-mixed redundancy strategy considering switching failure. Reliability Engineering and System Safety 2022; 228: 108814. https://doi.org/10.1016/j.ress.2022.108814
34. Lu C H, Gao Y, Cui Z W, Liu R G. Experimental analysis of chloride penetration into concrete subjected to drying-wetting cycle. Journal of Materials in Civil Engineering 2015; 27(12): 04015036. https://doi.org/10.1061/(ASCE)MT.1943-5533.0001304
35. Mangat P S, Molloy B T. Prediction of long term chloride concentration in concrete. Materials and Structures 1994; 27(6): 338-346. https://doi.org/10.1007/BF02473426
36. Marsh P S, Frangopol D M. Reinforced concrete bridge deck reliability model incorporating temporal and spatial variations of probabilistic corrosion rate sensor data. Reliability Engineering and System Safety 2008; 93: 394-409. https://doi.org/10.1016/j.ress.2006.12.011
37. Neuts M. Probability Distributions of Phase Type. E. H. Florin, Ed. Liber Amicorum, 1975.
38. Neuts M. Matrix-geometric solutions in stochastic models: an algorithmic approach. Baltimore, Md: Johns Hopkins University Press, 1981.
39. Okamura H, Dohi T, Osaki S. Software reliability growth models with normal failure time distributions. Reliability Engineering and System Safety 2013; 116: 135-141. https://doi.org/10.1016/j.ress.2012.02.002
40. Otieno M B, Beushausen H D, Alexander M G. Modelling corrosion propagation in reinforced concrete structures - A critical review. Cement and Concrete Composites 2011; 33(2): 240-245. https://doi.org/10.1016/j.cemconcomp.2010.11.002
41. Pack S W, Jung M S, Song H W, Kim S H, Ann K Y. Prediction of time dependent chloride transport in concrete structures exposed to a marine environment. Cement and Concrete Research 2010; 40(2): 302-312. https://doi.org/10.1016/j.cemconres.2009.09.023
42. Pugliese F, De Risi R, Di Sarno L. Reliability assessment of existing RC bridges with spatially-variable pitting corrosion subjected to increasing traffic demand. Reliability Engineering and System Safety 2022; 218: 108137. https://doi.org/10.1016/j.ress.2021.108137
43. Riascos-Ochoa J, Sanchez-Silva M, Akhavan-Tabatabaei R. Reliability analysis of shock-based deterioration using phase-type

distributions. Probabilistic Engineering Mechanics 2014; 38: 88-101. https://doi.org/10.1016/j.probengmech.2014.09.004

44. Saassouh B, Lounis Z. Probabilistic modeling of chloride-induced corrosion in concrete structures using first- and second-order reliability methods. Cement and Concrete Composites 2012; 34(9): 1082-1093. https://doi.org/10.1016/j.cemconcomp.2012.05.001
45. Shamstabar Y, Shahriari H, Samimi Y. Reliability monitoring of systems with cumulative shock-based deterioration process. Reliability Engineering and System Safety 2021; 216: 107937. https://doi.org/10.1016/j.ress.2021.107937
46. Shao W, Nie Y, Liang F, Shi D. A novel comprehensive evaluation method for the corrosion initiation life of RC hollow piles in chloride environments. Construction and Building Materials 2020; 249: 118801. https://doi.org/10.1016/j.conbuildmat.2020.118801
47. Shao W, Shi D, Tang P. Probabilistic Lifetime Assessment of RC Pipe Piles Subjected to Chloride Environments. Journal of Materials in Civil Engineering 2018; 30(11): 04018297. https://doi.org/10.1061/(ASCE)MT.1943-5533.0002512
48. Shim H S. Corner effect on chloride ion diffusion in rectangular concrete media. KSCE Journal of Civil Engineering 2002; 6: 19-24. https://doi.org/10.1007/BF02829036
49. Shuto S, Amemiya T. Sequential Bayesian inference for Weibull distribution parameters with initial hyperparameter optimization for system reliability estimation. Reliability Engineering and System Safety 2022; 224: 108516. https://doi.org/10.1016/j.ress.2022.108516
50. Stambaugh N D, Bergman T L, Srubar W V. Numerical service-life modeling of chloride-induced corrosion in recycled-aggregate concrete. Construction and Building Materials 2018; 161: 236-245. https://doi.org/10.1016/j.conbuildmat.2017.11.084
51. Steele C. Use of the lognormal distribution for the coefficients of friction and wear. Reliability Engineering and System Safety 2008; 93(10): 1574-1576. https://doi.org/10.1016/j.ress.2007.09.005
52. Stehlík M. Homogeneity and scale testing of generalized gamma distribution. Reliability Engineering and System Safety 2008; 93(12): 1809-1813. https://doi.org/10.1016/j.ress.2008.03.012
53. Sun B, Gardoni P. Directional search algorithm for hierarchical model development and selection. Reliability Engineering and System Safety 2019; 182: 194-207. https://doi.org/10.1016/j.ress.2018.09.013
54. Thomas M D A, Bamforth P B. Modelling chloride diffusion in concrete: Effect of fly ash and slag. Cement and Concrete Research 1999; 29(4): 487-495. https://doi.org/10.1016/S0008-8846(98)00192-6
55. Thummler A, Buchholz P, Telek M. A Novel Approach for Phase-Type Fitting with the EM Algorithm. IEEE Transactions on Dependable and Secure Computing 2006; 3(3): 245-258. https://doi.org/10.1109/TDSC.2006.27
56. Val D V, Trapper P A. Probabilistic evaluation of initiation time of chloride-induced corrosion. Reliability Engineering and System Safety 2008; 93: 364-372. https://doi.org/10.1016/j.ress.2006.12.010
57. Wang X, Ning R, Zhao X, Zhou J. Reliability analyses of k-out-of-n: F capability-balanced systems in a multi-source shock environment. Reliability Engineering and System Safety 2022; 227: 108733. https://doi.org/10.1016/j.ress.2022.108733
58. Wang X, Zhao X, Wu C, Wang S. Mixed shock model for multi-state weighted k-out-of-n: F systems with degraded resistance against shocks. Reliability Engineering and System Safety 2022; 217: 108098. https://doi.org/10.1016/j.ress.2021.108098
59. Wang Y, Wu L, Wang Y, Li Q, Xiao Z. Prediction model of long-term chloride diffusion into plain concrete considering the effect of the heterogeneity of materials exposed to marine tidal zone. Construction and Building Materials 2018; 159: 297-315. https://doi.org/10.1016/j.conbuildmat.2017.10.083
60. Weyers R E, Pyc W, Sprinkel M M, Kirkpatrick T J. Bridge deck cover depth specifications. Concrete International 2003; 25(2): 61-64.
61. Wu L, Li W, Yu X. Time-dependent chloride penetration in concrete in marine environments. Construction and Building Materials 2017; 152: 406-413. https://doi.org/10.1016/j.conbuildmat.2017.07.016
62. Xiao C. Corrosion of reinforcement in concrete and number theory simulation. Beijing: Tsinghua University, 1995.
63. Xu C, Wang C K, Jin W L. Interaction Effect of Chloride Attack and Carbonization in Concrete. Journal of Building Materials 2011; 14(3): 376-380. https://doi.org/10.3969/j.issn.1007-9629.2011.03.017
64. Xu D, Xiao X, Haibo Y. Reliability Evaluation of Smart Meters Under Degradation-Shock Loads Based on Phase-Type Distributions. IEEE Access 2020; 8: 39734-39746. https://doi.org/10.1109/ACCESS.2020.2976200
65. Yang Y, Li H. Time-dependent reliability calculation method of RC bridges based on the dual neural network. Soft Computing 2023; 27: 8855-8866. https://doi.org/10.1007/s00500-022-07763-9
66. Yao W, Chen X, Huang Y, van Tooren M. An enhanced unified uncertainty analysis approach based on first order reliability method with

single-level optimization. Reliability Engineering and System Safety 2013; 116: 28-37. https://doi.org/10.1016/j.ress.2013.02.014

67. Yeh W C. Novel self-adaptive Monte Carlo simulation based on binary-addition-tree algorithm for binary-state network reliability approximation. Reliability Engineering and System Safety 2022; 228: 108796. https://doi.org/10.1016/j.ress.2022.108796
68. Yu B, Ning C, Li B. Probabilistic durability assessment of concrete structures in marine environments: reliability and sensitivity analysis. China Ocean Engineering 2017; 31(1): 63-73. https://doi.org/10.1007/s13344-017-0008-3
69. Zhang H. Durability reliability analysis for corroding concrete structures under uncertainty. Mechanical Systems and Signal Processing 2018; 101: 26-37. https://doi.org/10.1016/j.ymssp.2017.08.027
70. Zhang X, Wang J, Zhao Y, Tang L, Xing F. Time-dependent probability assessment for chloride induced corrosion of RC structures using the third-moment method. Construction and Building Materials 2015; 76: 232-244. https://doi.org/10.1016/j.conbuildmat.2014.10.039
71. Zhang Z, Jiang C, Wang G G, Han X. First and second order approximate reliability analysis methods using evidence theory. Reliability Engineering and System Safety 2015; 137: 40-49. https://doi.org/10.1016/j.ress.2014.12.011